Progress in Nuclear Energy 143 (2022) 104036

Contents lists available at ScienceDirect

Progress in Nuclear Energy

journal homepage: www.elsevier.com/locate/pnucene

Gamma radiation shielding performance of $Cu_xAg_{(1-x)}$-alloys: Experimental, theoretical and simulation results

Mehmet Fatih Turhan [a,*], Ferdi Akman [b,c], Ahmet Taşer [d], Kamuran Dilsiz [e], Hasan Oğul [f], Mustafa Recep Kaçal [g], Osman Agar [h]

[a] Afyonkarahisar Health Sciences University, Atatürk Vocational School of Health Service, Department of Medical Imaging Techniques, 03200, Afyonkarahisar, Turkey
[b] Bingöl University, Vocational School of Social Sciences, Department of Property Protection and Security, Program of Occupational Health and Safety, 12000, Bingöl, Turkey
[c] Bingöl University, Central Laboratory Application and Research Center, 12000, Bingöl, Turkey
[d] Ağrı İbrahim Çeçen University, Patnos Vocational School, Departments of Medical Services and Techniques, Ağrı, Turkey
[e] Bingöl University, Faculty of Arts and Sciences, Department of Physics, 12000, Bingöl, Turkey
[f] Department of Nuclear Engineering, Faculty of Engineering and Architecture, Sinop University, Sinop, Turkey
[g] Giresun University, Arts and Sciences Faculty, Department of Physics, 28100, Giresun, Turkey
[h] Karamanoğlu Mehmetbey University, Department of Medical Imaging Techniques, 70100, Karaman, Turkey

ARTICLE INFO

Keywords:
Alloys
Gamma radiation attenuation
HPGe detector
FLUKA
GEANT4
WinXCOM

ABSTRACT

Different types of photon shielding parameters such as total mass attenuation coefficient (μ/ρ), linear attenuation coefficients (μ), half value layers (*HVL*), mean free paths (*MFP*), effective atomic numbers (Z_{Eff}), energy absorption build-up factors (*EABF*), exposure build-up factors (*EBF*) and kerma relative to air were investigated for the fabricated Cu–Ag based alloys. The considered parameters were measured through gamma spectrometer equipped with HPGe detector in order to obtain the experimental attenuation coefficients and other related parameters at various photon energy in the energy range 59.5–1332.5 keV. The measured μ/ρ values were confirmed with WinXCOM database results. FLUKA and GEANT4 simulation codes were used to examine the compatibility of the experimental and WinXCOM database results with these simulation codes. The exposure buildup factors of the alloy samples were estimated with help of Geometric Progression fitting formula over photon energy 0.015–15 MeV up to 40 *mfp* penetration depth. The results revealed that the exhibited effectiveness of $Cu_{0.2}Ag_{0.8}$ alloys against high energetic photon radiations had a good performance than that of alternative absorbers such conventional concretes, glasses and some alloys. The results of the present survey can be quite useful for possible applications of such materials, especially in nuclear laboratory and reactor core design for preference of effective photon shielding materials.

1. Introduction

The use of nuclear energy as an alternative energy source is quite effective way in terms of energy diversity and decreasing the environmental impacts of energy production (Majid et al., 2013; Kok and Benli, 2017). Considering the fact that its negative effects are lesser than those other sources, it could be considered among the best choices for the current and future energy demands. On the other hand, high-energetic X-/gamma ray radiations, which are associated with nuclear energy, is one of great deal practices such as diagnostics (Suortti and Thomlinson, 2003), elemental analysis by photoactivation (Boztosun et al., 2014), nuclear structure (Agar et al., 2017). High energetic photons are widely utilized in medicine (radiotherapy), industry (sterilization and disinfection) and the nuclear industry due to having the smallest wavelengths and the most energy of any other wave in the electromagnetic spectrum.

One of the most fundamental issues to be considered and addressed is the protection of people working in these areas or the electronic devices in these environments from the harmful effects of such ionizing radiations. Decreasing the harmful radiation impacts and avoiding radiation risk are adopted As Low As Reasonably Achievable (ALARA) rules, which mean that even the lowest dose should be avoided if it is not necessary (Tekin and Kilicoglu, 2020). ALARA can be employed by ways of three safety principles namely time, distance and shielding. Among them, the shielding is the most effective technique due to the flexibility

* Corresponding author.
E-mail address: m.f.turhan@hotmail.com (M.F. Turhan).

https://doi.org/10.1016/j.pnucene.2021.104036
Received 11 June 2021; Received in revised form 22 September 2021; Accepted 1 November 2021
Available online 8 November 2021

Table 1
Detail information of the synthesized alloys.

Sample	Composition (%)		Weight fraction		Density (g/cm^3)
	Cu	Ag	Cu	Ag	
$Cu_{0.2}Ag_{0.8}$	20	80	0.314733	0.741646	10.2954
$Cu_{0.4}Ag_{0.6}$	40	60	0.629465	0.556234	10.0271
$Cu_{0.5}Ag_{0.5}$	50	50	0.786832	0.463529	9.6571
$Cu_{0.6}Ag_{0.4}$	60	40	0.944198	0.370823	9.4376
$Cu_{0.8}Ag_{0.2}$	80	20	1.258931	0.185411	9.1580

and liberty for material choice on stopping/attenuating the hazardous radiations. Lead (Pb) and traditional heavy concretes which are materials with high atomic number (Z) are generally utilized to provide a shelter from penetrative radiations such as nuclear power plants. However, Pb has some drawbacks such as toxicity, being heavy, difficulties on the processing and moving from one place to another (Eke et al., 2017) while there is inverse proportionality between tensile strength and radiation shielding performance of concretes containing heavy element (Kaur et al., 2019). Various new materials have been sought in order to obtain alternative shielding materials to traditional absorbers such as glasses (Aygün et al., 2020), ceramics (Sayyed et al., 2018; Akman et al., 2019a), green product (Akman et al., 2019b), composites (Akman et al., 2021a, 2021b, 2021c) and etc.

Alloys are the most outstanding and remarkable materials in order to minimize the dose level in high-radiation mediums and be used in nuclear power facilities. Any alloys can be obtained by composing two or more elements together with a motive to develop mechanical and physical features such as ductility, creep resistance, tensile strength, elastic modulus and hardness as compared to its parent elements (Ahmed and Flower, 1992; Moiseev et al., 1998; Kamal et al., 2006). Recently, some researchers have explored the potentiality of different alloys such as fusible (Singh et al., 2018), Pd–Ag binary (Agar et al., 2019), Cerrobend (Tellili et al., 2017), Fe–B (Levent et al., 2020), Fe–Cr–Ni (Akman et al., 2019c), $Fe_xSe_{0.5}Te_{0.5}$ (Hamad et al., 2021), Sn–Bi based alloys (Reda and El-Daly, 2020) as gamma rays shielding material.

In this context, copper - silver (Cu–Ag) binary alloys are of scientific interest and recently, used in numerous fields such as costume, jewelry, coins, musical instruments, radiators, dental casting, electronics, springs etc. Cu–Ag alloys are generally used in micro-device technologies where properties such as conductivity, strength and magnetism are active. Also, Cu–Ag alloys can be used in micro-devices exposed to radiation with their radiation attenuation feature and alternatively as radiation shielding material in health areas. The other important specification of Cu based alloys are that they are resistant to corrosion in varied atmospheres (Kaur et al., 2019). The insertion of Cu to Ag enhances its hardness, increases its melting point, and increases its nobility and resistance to tarnishing. Since there is difference of 18 between the atomic number of constituent elements: Cu (Z = 29) and Ag (Z = 47); a systematical approach has been studied the amount effect of Cu on some radiation attenuation parameters. Therefore, five samples of $Cu_xAg_{(1-x)}$ were fabricated, where x varies between x = 0.2, 0.4, 0.5, 0.6 and 0.8.

Here, the main aim of this work is to reveal the relationship between various types of Ag–Cu based alloys which have Z atomic number compared to other light atoms and their nuclear properties for the probabilities of their use in different places in nuclear reactors systems as well as show the utilization in various purposes such as nuclear research laboratory, oncology department at hospital, nuclear plants and other radiation related fields. The X-ray and gamma radiation shielding parameters such as mass attenuation coefficients, linear attenuation coefficients, half value layer, mean free paths, effective atomic numbers, exposure buildup factors, and kerma (kinetic energy released per unit mass) relative to air for Cu–Ag alloys have been studied. The experimental data have been approved with those of theoretical (WinXCOM) and simulation (FLUKA and GEANT4 codes) ones.

2. Material and method

2.1. Sample preparation

On the first step, Cu and Ag metals were weighed with a scale with 0.0001 precision to obtain $Cu_{0.2}Ag_{0.8}$, $Cu_{0.4}Ag_{0.6}$, $Cu_{0.5}Ag_{0.5}$ $Cu_{0.6}Ag_{0.4}$ and $Cu_{0.8}Ag_{0.2}$ by weight ratio of CuAg alloys. Each produced metal was washed in acetone, methanol and trichlorethylene respectively for 30 s in an ultrasonic bath and then dried using nitrogen gas (99.999% purity). The dried metals were washed in diluted HCl solution (H_2O: HCl; 10: 1) for 30 s in an ultrasonic bath. It was then washed thoroughly with deionized water and dried again with pure nitrogen gas. Thus, various organic and inorganic dirt and oxide layers on the surfaces of metals were removed from the surfaces. On the second step, the internal setup of the thermal evaporation system that we will use to alloy the metals has been prepared. First, a molybdenum plate is placed between the electrodes. Secondly, the quartz crucible, which was cleaned and dried beforehand, is placed on the molybdenum plate. Thirdly, the alloy metals prepared beforehand are placed in the quartz crucible and the thermal evaporation system is put into vacuum and a pressure of 10^{-7} torr is expected to decrease. Finally, when the thermal evaporation system reaches 10^{-7} torr pressure, the quartz crucible is heated by gradually giving current to the electrodes and by looking at the control window of the thermal evaporation system, the metals in the quartz crucible are expected to become alloy. These processes were carried out in pre-weighed and prepared other metals, and alloys with weight ratios $Cu_{0.2}Ag_{0.8}$, $Cu_{0.4}Ag_{0.6}$, $Cu_{0.5}Ag_{0.5}$ $Cu_{0.6}Ag_{0.4}$ and $Cu_{0.8}Ag_{0.2}$ were obtained. The thicknesses of the alloys were in the range between 0.318 and 0.454 cm. The composition and densities of the fabricated alloys are given in Table 1.

2.2. Gamma ray transmission measurement

Am-241 (460 kBq), Na-22 (456 kBq), Mn-54 (378 kBq), Co-57 (413 kBq), Co-60 (424 kBq), Ba-133 (460 kBq) and Cs-137 (473 kBq) radiation sources were used in transmission measurements. Photons passing through the alloys were detected by HPGe detector with a resolution of 380 eV at 5.9 keV, 585 eV at 122 keV and 1.8 keV at 1.33 MeV. The detector was encircled with a collimator manufactured from Pb, Fe, and Al, to minimize the effects from the environment (Sharma et al., 2020; Kaçal et al., 2020; Akman et al., 2020). The experimental arrangement is shown in Fig. 1. The photons passing through the alloys were counted 1000 s to obtain sufficient statistical accuracy. Peak areas were investigated with the Microcal Origin 7.5 (Akman et al., 2018) demo version software program. In the experiment, the alloys were measured at 13 different energies (59.5 keV $\leq$ E $\leq$ 1332.5 keV) in the transmission geometry and the attenuation and related parameters were evaluated with the help of these measurements.

2.3. Photon shielding parameters

Total mass attenuation coefficient is defined the following equation (Almatari et al., 2019);

$$\frac{\mu}{\rho} = \frac{1}{\rho x}\ln\left(\frac{I}{I_0}\right) \quad (1)$$

I and I_0 represent transmitted intensity and the primary intensity, respectively. μ, ρ, and x corresponds to the linear attenuation coefficient, the density of the absorber, and the thickness of the absorber, respectively.

Total mass attenuation coefficient of the any alloy, mixture or compound is computed using the mixture rule ($(\mu/\rho)_{Comp} = \sum W_i(\mu/\rho)_i$)

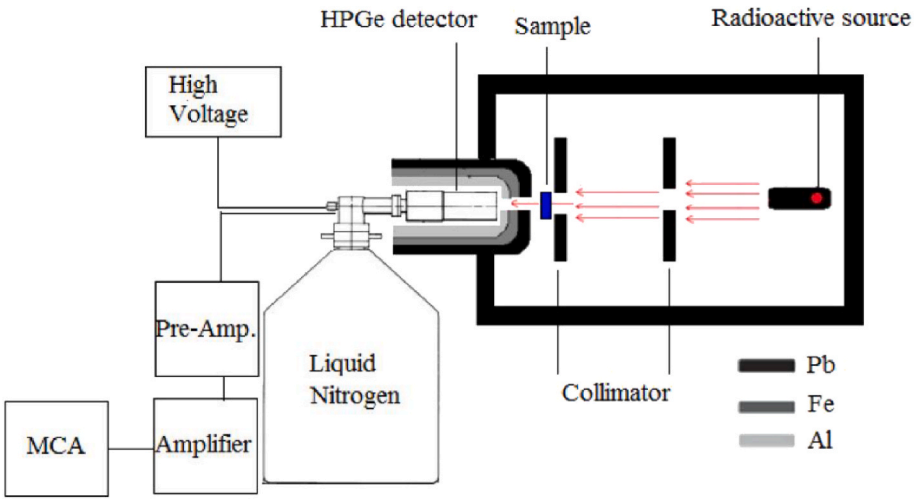

Fig. 1. The designed experimental geometry to determine gamma radiation shielding properties.

Table 2
The mass attenuation coefficient ($cm^2\ g^{-1}$) values of Cu–Ag alloys obtained by experimental, theoretical and simulations.

Energy (keV)	$Cu_{0.2}Ag_{0.8}$				$Cu_{0.4}Ag_{0.6}$				$Cu_{0.5}Ag_{0.5}$			
	Exp.	WinX.	GEANT	FLUKA	Exp.	WinX.	GEANT	FLUKA	Exp.	WinX.	GEANT	FLUKA
59.5	5.0791 ± 0.0542	4.9180	4.8025	5.0686	4.4890 ± 0.0483	4.3078	3.9770	4.2933	3.7334 ± 0.0412	3.5824	3.5606	3.7592
81.0	2.0911 ± 0.0248	2.1490	2.0686	2.2000	1.8233 ± 0.0226	1.8879	1.7196	1.8355	1.6031 ± 0.0227	1.5775	1.5460	1.6314
122.1	0.7629 ± 0.0397	0.7542	0.7098	0.7694	0.6622 ± 0.0392	0.6717	0.6019	0.6548	0.5411 ± 0.0314	0.5738	0.5477	0.5784
276.4	0.1691 ± 0.0079	0.1616	0.1513	0.1627	0.1442 ± 0.0077	0.1536	0.1409	0.1517	0.1363 ± 0.0077	0.1441	0.1364	0.1462
302.9	0.1392 ± 0.0092	0.1443	0.1360	0.1449	0.1343 ± 0.0077	0.1382	0.1276	0.1368	0.1331 ± 0.0080	0.1309	0.1241	0.1321
356.0	0.1263 ± 0.0065	0.1213	0.1140	0.1218	0.1145 ± 0.0064	0.1175	0.1094	0.1163	0.1171 ± 0.0065	0.1129	0.1075	0.1137
383.9	0.1166 ± 0.0044	0.1129	0.1068	0.1132	0.1045 ± 0.0044	0.1098	0.1034	0.1090	0.1002 ± 0.0048	0.1062	0.1015	0.1069
511.0	0.0844 ± 0.0039	0.0896	0.0870	0.0895	0.0839 ± 0.0041	0.0883	0.0851	0.0879	0.0879 ± 0.0046	0.0868	0.0847	0.0867
661.7	0.0795 ± 0.0039	0.0755	0.0741	0.0751	0.0759 ± 0.0043	0.0749	0.0733	0.0745	0.0773 ± 0.0042	0.0743	0.0732	0.0742
834.8	0.0689 ± 0.0038	0.0657	0.0652	0.0652	0.0618 ± 0.0037	0.0655	0.0647	0.0652	0.0681 ± 0.0039	0.0653	0.0650	0.0651
1173.2	0.0520 ± 0.0020	0.0541	0.0545	0.0540	0.0553 ± 0.0021	0.0541	0.0539	0.0540	0.0514 ± 0.0022	0.0542	0.0538	0.0539
1274.5	0.0486 ± 0.0026	0.0517	0.0522	0.0516	0.0536 ± 0.0027	0.0518	0.0517	0.0517	0.0533 ± 0.0027	0.0519	0.0518	0.0517
1332.5	0.0477 ± 0.0023	0.0505	0.0504	0.0506	0.0536 ± 0.0021	0.0506	0.0506	0.0505	0.0511 ± 0.0023	0.0507	0.0505	0.0507

Energy (keV)	$Cu_{0.6}Ag_{0.4}$				$Cu_{0.8}Ag_{0.2}$			
	Exp.	WinX.	GEANT	FLUKA	Exp.	WinX.	GEANT	FLUKA
59.5	3.0969 ± 0.0334	3.1658	3.1486	3.1812	2.5663 ± 0.0284	2.4575	2.3253	2.4788
81.0	1.4486 ± 0.0183	1.3993	1.3705	1.4710	1.1281 ± 0.0168	1.0963	1.0216	1.1063
122.1	0.5382 ± 0.0313	0.5175	0.4944	0.5400	0.4079 ± 0.0221	0.4219	0.3855	0.4248
276.4	0.1329 ± 0.0056	0.1386	0.1311	0.1403	0.1237 ± 0.0068	0.1293	0.1215	0.1295
302.9	0.1301 ± 0.0070	0.1267	0.1201	0.1282	0.1151 ± 0.0064	0.1196	0.1131	0.1197
356.0	0.1121 ± 0.0052	0.1103	0.1052	0.1113	0.1077 ± 0.0063	0.1058	0.1005	0.1058
383.9	0.0985 ± 0.0035	0.1041	0.0998	0.0956	0.0960 ± 0.0039	0.1005	0.0964	0.1004
511.0	0.0863 ± 0.0032	0.0859	0.0838	0.0863	0.0827 ± 0.0038	0.0844	0.0827	0.0844
661.7	0.0715 ± 0.0034	0.0739	0.0727	0.0741	0.0746 ± 0.0038	0.0733	0.0723	0.0731
834.8	0.0622 ± 0.0031	0.0651	0.0647	0.0650	0.0631 ± 0.0034	0.0649	0.0648	0.0646
1173.2	0.0514 ± 0.0017	0.0542	0.0539	0.0541	0.0551 ± 0.0019	0.0543	0.0542	0.0542
1274.5	0.0540 ± 0.0022	0.0519	0.0519	0.0519	0.0496 ± 0.0025	0.0520	0.0519	0.0518
1332.5	0.0497 ± 0.0018	0.0507	0.0505	0.0507	0.0484 ± 0.0021	0.0508	0.0508	0.0507

and comprehensive clarification of the mixture rule used has been already discussed in our previous work (Kaçal et al., 2020). Linear attenuation coefficient can be determined by the mass attenuation coefficient and physical density of alloy. Half Value Layer (*HVL*) and Mean Free Path (*MFP*) are described the thickness of sample required to reduce photon intensity to 1/2 and the average distance between two consecutive collisions, respectively. *HVL* and *MFP* are associated to linear attenuation coefficient, and they could be determined using Eq. (2), Eq. (3), respectively (Sayyed et al., 2020).

$$HVL = \frac{\ln 2}{\mu} \tag{2}$$

$$MFP = \frac{1}{\mu} \tag{3}$$

Eq. (4) describes the effective atomic number, respectively (Sayyed et al., 2019).

$$Z_{Eff} = \frac{\sum_i f_i A_i \left(\mu/\rho\right)_i}{\sum_j f_j^{\frac{A_j}{Z_j}} \left(\mu/\rho\right)_j} \tag{4}$$

where, f_i represents the fractional abundance of the relative element in the material, A_i and Z_j represent the atomic weight and atomic number.

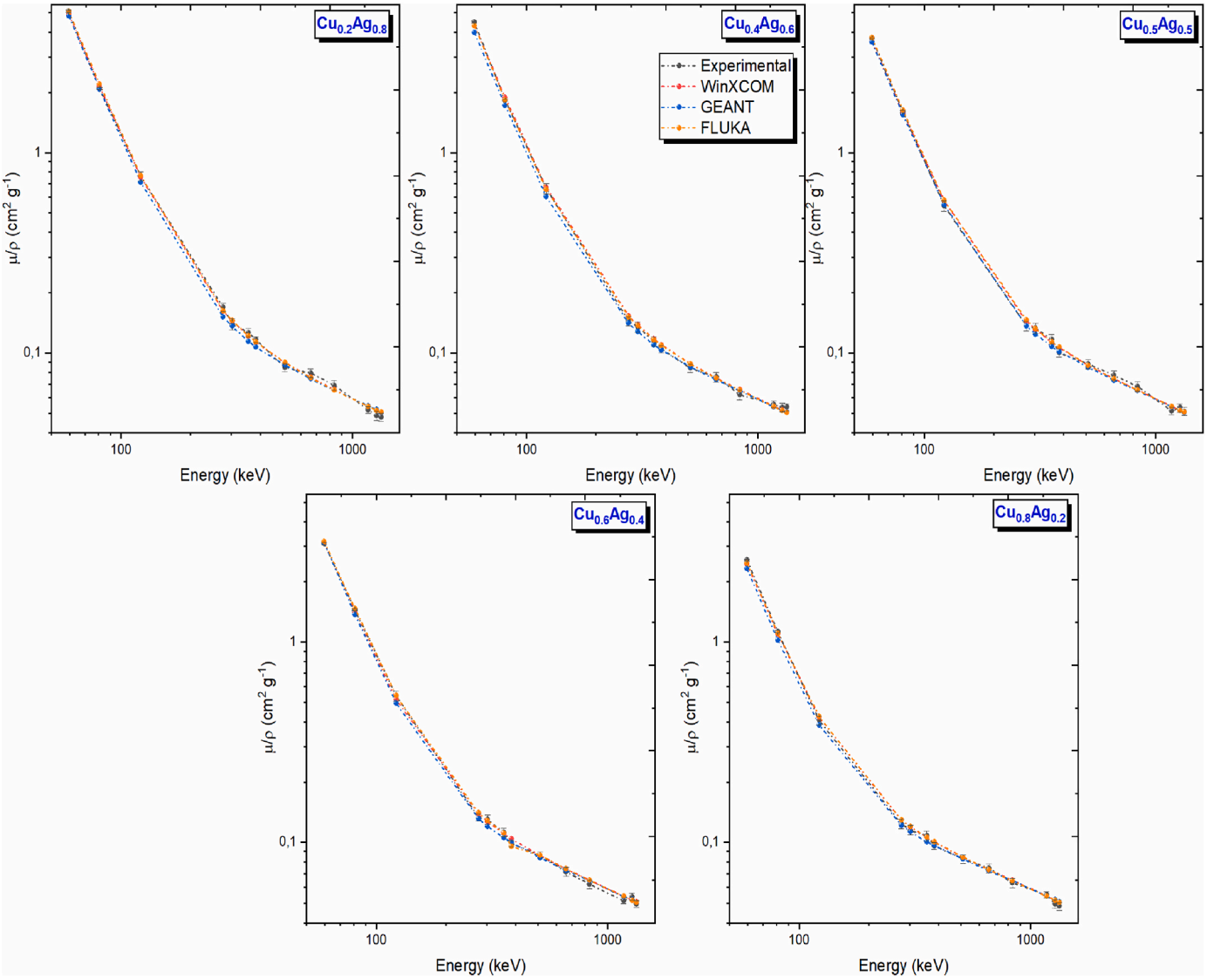

Fig. 2. The experimental, WinXCOM, GEANT and FLUKA mass attenuation coefficient results for manufactured alloys.

Table 3
The linear attenuation coefficient (cm^{-1}) values of Cu–Ag alloys obtained by experimental and theoretical.

Energy (keV)	$Cu_{0.2}Ag_{0.8}$		$Cu_{0.4}Ag_{0.6}$		$Cu_{0.5}Ag_{0.5}$		$Cu_{0.6}Ag_{0.4}$		$Cu_{0.8}Ag_{0.2}$	
	Exp.	Theo.	Exp.	Theo.	Exp.	Theo.	Exp.	Theo.	Exp.	Theo.
59.5	52.291 ± 0.558	50.633	45.012 ± 0.484	43.195	36.054 ± 0.398	34.595	29.228 ± 0.315	29.878	23.502 ± 0.260	22.506
81.0	21.529 ± 0.255	22.124	18.283 ± 0.226	18.930	15.481 ± 0.219	15.234	13.672 ± 0.173	13.206	10.331 ± 0.154	10.040
122.1	7.854 ± 0.408	7.764	6.640 ± 0.393	6.736	5.225 ± 0.303	5.541	5.080 ± 0.295	4.884	3.735 ± 0.202	3.864
276.4	1.741 ± 0.081	1.663	1.446 ± 0.077	1.540	1.316 ± 0.074	1.391	1.255 ± 0.053	1.308	1.133 ± 0.063	1.184
302.9	1.433 ± 0.095	1.486	1.346 ± 0.077	1.386	1.285 ± 0.077	1.264	1.228 ± 0.066	1.196	1.054 ± 0.058	1.095
356.0	1.300 ± 0.067	1.249	1.148 ± 0.064	1.178	1.131 ± 0.063	1.090	1.058 ± 0.049	1.041	0.987 ± 0.058	0.969
383.9	1.200 ± 0.045	1.162	1.048 ± 0.044	1.101	0.967 ± 0.046	1.025	0.930 ± 0.033	0.982	0.880 ± 0.035	0.920
511.0	0.869 ± 0.041	0.923	0.842 ± 0.041	0.886	0.849 ± 0.044	0.838	0.814 ± 0.030	0.811	0.758 ± 0.035	0.773
661.7	0.818 ± 0.040	0.777	0.761 ± 0.043	0.751	0.746 ± 0.040	0.718	0.675 ± 0.032	0.698	0.683 ± 0.035	0.672
834.8	0.709 ± 0.039	0.676	0.620 ± 0.037	0.656	0.657 ± 0.038	0.630	0.587 ± 0.029	0.615	0.578 ± 0.031	0.595
1173.2	0.535 ± 0.021	0.557	0.555 ± 0.021	0.543	0.496 ± 0.021	0.523	0.485 ± 0.016	0.512	0.505 ± 0.017	0.497
1274.5	0.500 ± 0.027	0.532	0.537 ± 0.027	0.519	0.515 ± 0.026	0.501	0.510 ± 0.021	0.490	0.455 ± 0.023	0.476
1332.5	0.491 ± 0.024	0.520	0.538 ± 0.021	0.507	0.493 ± 0.023	0.490	0.469 ± 0.017	0.479	0.443 ± 0.019	0.466

2.4. Theoretical and simulation calculations

Monte Carlo Simulations have vital contributions to both experimental and theoretical researches, and various simulation codes are in use to validate experimental designs and results. Their usage differs based on the aim of the study, and proper simulation tools are needed to be chosen for the intended work. In this context, WinXCOM (Gerward et al., 2004), GEANT4 (Agostinelli et al., 2003) and FLUKA (Böhlen et al., 2014) are some of excellent codes to evaluate the materials' gamma attenuation characteristics, that are already proven by many

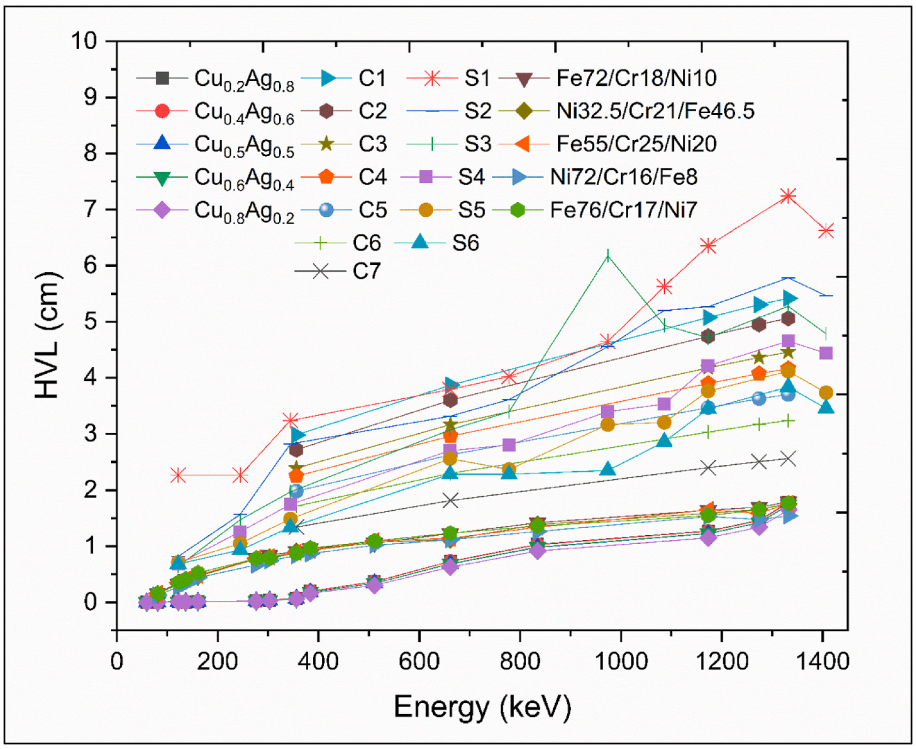

Fig. 3. The theoretical half value layer results for the studied alloys.

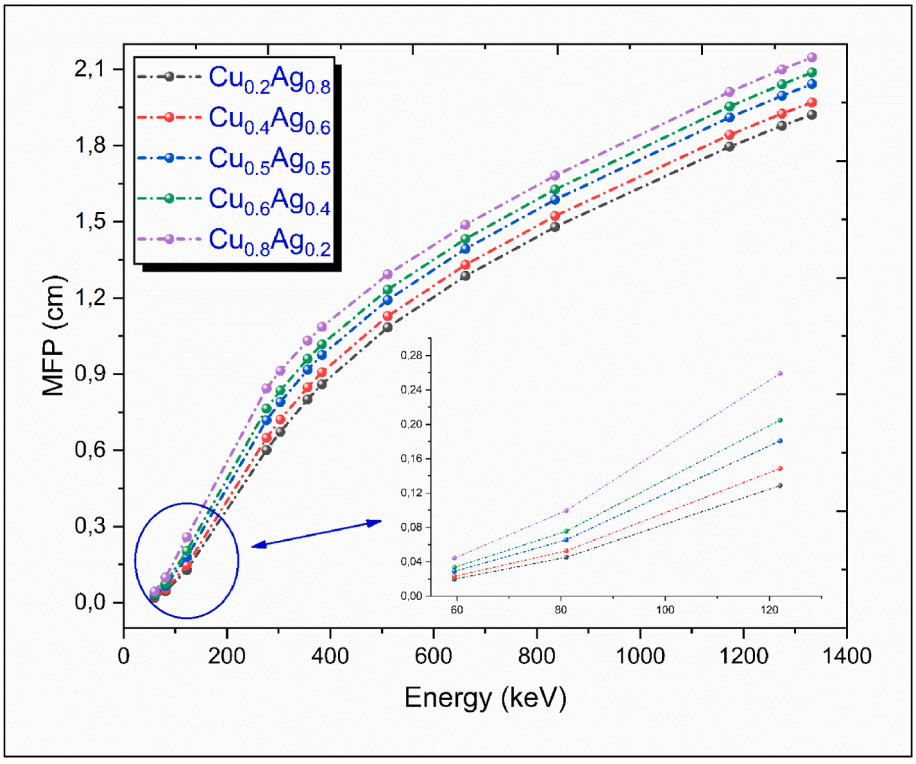

Fig. 4. The theoretical mean free path results for the prepared alloys.

studies (Elbashir et al., 2018; Kurtulus et al., 2021; Al-Buriahi and Singh, 2020; Taqi et al., 2021; Al-Buriahi et al., 2021; Aşkin et al., 2020). It should be noted here that, WinXCOM is a database tool to calculate theoretical attenuation coefficients while GEANT4 and FLUKA are the simulation tools.

In this work, the chosen alloys were defined in WinXCOM database tool and the simulation tools of GEANT4 and FLUKA with help of their chemical compositions. The database and simulation codes consider the homogenous mixture of the samples. A wide gamma energy range, varying from 59.5 keV to 1332.5 keV, is taken into account, and the

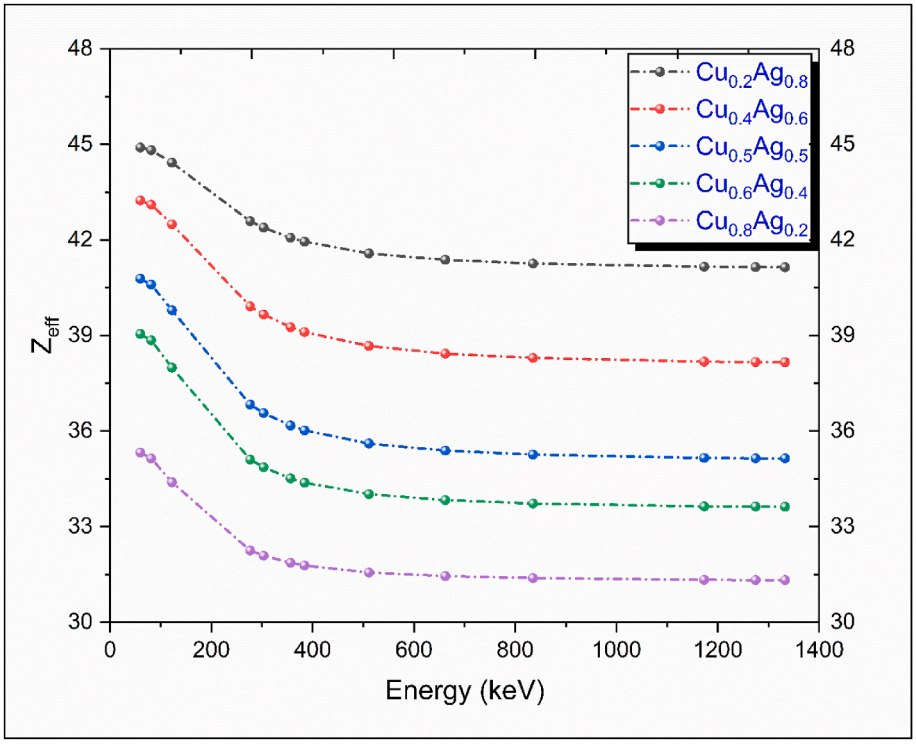

Fig. 5. The theoretical effective atomic number results for the present alloys.

Table 4
Equivalent atomic numbers of alloys for the energy range from 0.015 to 15 MeV.

Energy (MeV)	$Cu_{0.2}Ag_{0.8}$	$Cu_{0.4}Ag_{0.6}$	$Cu_{0.5}Ag_{0.5}$	$Cu_{0.6}Ag_{0.4}$	$Cu_{0.8}Ag_{0.2}$
0.015	36.490	36.450	36.408	36.387	36.354
0.02	42.747	42.703	42.658	42.635	42.599
0.03	43.324	41.007	38.133	36.387	33.236
0.04	43.551	41.274	38.421	36.675	33.459
0.05	43.669	41.435	38.603	36.858	33.601
0.06	43.737	41.541	38.733	36.989	33.703
0.08	43.821	41.672	38.891	37.151	33.834
0.1	43.891	41.762	39.000	37.265	33.928
0.15	43.988	41.906	39.180	37.446	34.094
0.2	44.049	41.994	39.293	37.565	34.194
0.3	44.114	42.102	39.424	37.700	34.309
0.4	44.163	42.171	39.508	37.788	34.389
0.5	44.189	42.206	39.556	37.843	34.432
0.6	44.199	42.225	39.587	37.878	34.464
0.8	44.215	42.253	39.618	37.911	34.492
1	44.222	42.264	39.628	37.920	34.503
1.5	44.036	41.957	39.195	37.434	34.034
2	43.609	41.273	38.329	36.532	33.260
3	43.110	40.606	37.569	35.786	32.709
4	42.935	40.357	37.303	35.531	32.521
5	42.830	40.237	37.164	35.397	32.428
6	42.791	40.166	37.081	35.338	32.411
8	42.698	40.056	36.977	35.237	32.334
10	42.649	40.005	36.934	35.191	32.316
15	42.633	39.951	36.901	35.158	32.296

same energy values were used in both simulation and experimental calculations for the consistency. WinXCOM tool directly provides μ/ρ value for the corresponding energy in the unit of cm^2/g once the chemical compositions of the alloy and the desired energy are encoded. From there, the remaining parameters could be easily calculated. On the other hand, GEANT4 and FLUKA codes require the parameterization of the samples with their sizes and densities in addition to their chemical compositions. In both GEANT4 and FLUKA, the modelled and defined samples were bombarded with 10 000 000 gammas at the desired particle energy in order to obtain the attenuation coefficients and remaining related parameters. The obtained precise numerical values were further used in the evaluation of the experimental outcomes.

2.5. Calculation procedure of energy absorption and exposure build-up factors

In order to calculate the build-up factor using geometric progression (G-P) fitting method, firstly equivalence atomic number (Z_{eq}) is calculated and after that G-P fitting coefficients determined using the Z_{eq}. Finally, build-up factors are obtained with the help of the G-P fitting coefficients. These steps are detailed below.

In order to determine Z_{eq}, Compton partial mass attenuation coefficient ($(\mu/\rho)_{Compton}$) and total mass attenuation coefficient ($(\mu/\rho)_{Total}$) were determined using the WinXCOM for both elements in the atomic number range from 32 to 45 and alloys in the energy 0.015 MeV $\leq$ E $\leq$ 15 MeV. Z_{eq} is computed by matching the ratio of $(\mu/\rho)_{Compton}$ to $(\mu/\rho)_{Total}$ of the specific energy for both alloy and an element. When the ratio of $(\mu/\rho)_{Compton}$ to $(\mu/\rho)_{Total}$ lies among two consecutive ratios of elements for an alloy, the interpolation of the Z_{eq} of an alloy is determined as follow.

$$Z_{eq} = \frac{Z_1(\log R_2 - \log R) + Z_2(\log R - \log R_1)}{\log R_2 - \log R_1} \quad (5)$$

R_1, R_2 and R are the ratio for the two consecutive elements and alloy at specific energy, respectively. Z_1 and Z_2 are the atomic numbers of the corresponding elements.

Geometric progression (G-P) fitting coefficients for an alloy were calculated by the interpolation procedure similar to the equivalent atomic number calculation procedure. G-P fitting coefficients (b, c, a, X_k and d) are determined using Eq. (6).

$$P = \frac{P_1(\log Z_2 - \log Z_{eq}) + P_2(\log Z_{eq} - \log Z_1)}{\log Z_2 - \log Z_1} \quad (6)$$

P_1 and P_2 are the G-P fitting coefficients of the corresponding elements at a given energy. The G-P fitting coefficients for elements were

Table 5
G-P energy absorption and exposure build-up factor parameters of the $Cu_{0.4}Ag_{0.6}$ in the energy range from 0.015 MeV to 15 MeV.

Energy (MeV)	*EABF*					*EBF*				
	a	b	c	d	X_k	a	b	c	d	X_k
0.015	0.005	1.006	1.017	0.045	13.132	0.019	1.006	1.008	0.029	12.057
0.02	0.039	1.206	1.885	−0.016	17.659	0.039	2.409	1.871	−0.018	13.391
0.03	0.115	1.482	1.053	−0.123	26.928	0.115	3.473	1.045	−0.207	30.839
0.04	0.111	1.468	0.323	−0.056	23.325	0.095	3.805	0.322	−0.035	22.950
0.05	−0.139	1.372	0.063	0.112	8.468	−0.297	3.035	0.050	0.049	11.994
0.06	0.783	1.321	0.032	−0.190	14.899	1.077	2.369	0.015	−0.148	17.402
0.08	0.565	1.299	0.088	−0.226	14.047	0.755	1.651	0.042	−0.253	14.391
0.1	0.325	1.197	0.257	−0.167	13.876	0.288	1.160	0.303	−0.154	13.752
0.15	0.287	1.451	0.322	−0.159	14.096	0.174	1.243	0.491	−0.090	14.417
0.2	0.318	2.280	0.307	−0.199	14.030	0.173	1.474	0.514	−0.099	14.290
0.3	0.160	2.379	0.558	−0.098	14.057	0.080	1.586	0.732	−0.043	14.486
0.4	0.107	2.668	0.711	−0.087	13.909	0.039	1.707	0.889	−0.034	14.179
0.5	0.068	2.687	0.827	−0.065	13.899	0.017	1.768	0.975	−0.024	14.322
0.6	0.048	2.644	0.888	−0.054	13.759	0.005	1.791	1.021	−0.019	13.942
0.8	0.026	2.499	0.963	−0.040	13.659	−0.007	1.800	1.070	−0.013	14.022
1	0.015	2.365	0.998	−0.032	13.548	−0.013	1.780	1.090	−0.011	13.430
1.5	−0.011	1.941	1.093	−0.015	13.455	−0.030	1.624	1.161	0.001	7.161
2	0.001	1.849	1.051	−0.023	12.901	−0.021	1.605	1.127	−0.005	12.445
3	0.031	1.716	0.964	−0.053	13.124	0.000	1.562	1.064	−0.027	12.783
4	0.049	1.594	0.918	−0.070	13.580	0.015	1.509	1.023	−0.041	13.313
5	0.076	1.556	0.852	−0.095	13.823	0.042	1.514	0.950	−0.066	13.552
6	0.087	1.498	0.832	−0.104	14.036	0.053	1.489	0.930	−0.074	13.749
8	0.101	1.456	0.813	−0.115	14.259	0.075	1.508	0.888	−0.093	14.067
10	0.081	1.388	0.889	−0.095	14.347	0.057	1.474	0.965	−0.076	14.171
15	0.062	1.370	1.008	−0.082	14.352	0.037	1.521	1.098	−0.060	14.203

taken from the ANSI/ANS-6.4.3 (1991) standard reference database.

Finally, the energy absorption build-up factor (*EABF*) and exposure build-up factor (*EBF*) are determined using the G-P fitting coefficients as follow;

$$B(E,x) = 1 + \frac{b-1}{K-1}(K^x - 1)\ for\ K \neq 1 \tag{7}$$

$$B(E,x) = 1 + (b-1)x\ for\ K = 1 \tag{8}$$

where,

$$K(E,x) = cx^a + d\frac{\tanh(x/X_k - 2) - \tanh(-2)}{1 - \tanh(-2)}\ for\ x \leq 40\ mfp \tag{9}$$

the incident photon energy is represented by E; the penetration depth in *mfp* is represented by x; the G-P fitting coefficients are symbolized with b, c, a, X_k and d, the value of build-up factor at 1 *mfp* is represented by b.

2.6. Calculation procedure of kerma relative to air

Kerma relative to air values of an alloy can be computed using the following equation.

$$\frac{(\mu_{en}/\rho)_{Alloy}}{(\mu_{en}/\rho)_{Air}} \tag{10}$$

The mass energy absorption coefficient for an alloy is determined with the help of Eq (11).

$$\left(\frac{\mu_{en}}{\rho}\right)_{Alloy} = \sum W_i \left(\frac{\mu_{en}}{\rho}\right)_i \tag{11}$$

where, the weight fraction is symbolized with W_i and the mass energy absorption coefficient of the ith constituent element is symbolized with $(\mu_{en}/\rho)_i$. Mass energy absorption coefficients taken from Hubbell and Seltzer (1995).

$$W_i = \frac{n_i A_i}{\sum_j n_j A_j} \tag{12}$$

A_i is the atomic weight of the ith element and n_i imply the number of atoms of ith constituent element in alloy.

3. Results and discussions

3.1. Photon shielding parameters

In this study, radiation shielding features were investigated for $Cu_{0.2}Ag_{0.8}$, $Cu_{0.4}Ag_{0.6}$, $Cu_{0.5}Ag_{0.5}$, $Cu_{0.6}Ag_{0.4}$ and $Cu_{0.8}Ag_{0.2}$. These alloys were manufactured with different amounts of Ag and Cu elements and the percentages of Ag and Cu elements in the alloys were given along with weight fractions and densities in Table 1. The shielding characteristics of the manufactured alloys were tested by measuring the quantities such as mass and linear attenuation coefficients and etc. Table 2 shows μ/ρ values of experimental, theoretical and simulation results for five different samples. These results were obtained using a gamma source with the energies ranged from 59.5 to 1332.5 keV. A comparison of these results was plotted in Fig. 2. As can be seen, experimental results are supremely consistent with theoretical WinXCOM and simulation (GEANT4 and FLUKA) results. This consistency shows the accuracy and satisfaction of experimental design for determining the shielding effect of the manufactured alloys. The results in Table 2 also show that the mass attenuation values of $Cu_{0.2}Ag_{0.8}$ alloy were found to be greater than the mass attenuation results of the other four samples at low energies. However, this difference decreases while the energy is increased.

Additionally, the μ/ρ values of the investigated alloy samples diminish rapidly throughout the low energy region for less than 303 keV while getting slight with increasing of energy (E > 303 keV). The basic reason of this difference is that two photon interaction modes happen in different regions. In short, one of both, the photoelectric (PE) absorption is the most dominant interaction process over 59.5 keV < E < 303 keV as compared to Compton scattering (CS) processes, where is more dominant for E > 303 keV. Both processes are resultant from the energy as $E^{-3.5}$ and E^{-1}, respectively. Moreover, the above-mentioned quick and linear reductions are highly related to the dependence of PE and CS with the atomic number as Z^{4-5} and Z, respectively. Systematically, these physical behaviors overlap with the observed alteration in μ_m values published by Kacal et al. (2021).

Investigation of μ parameter of the prepared alloys is important to test the shielding property since several quantities such as *HVL*, *MFP*, Z_{eff} and etc., could be obtained with the use of the linear attenuation

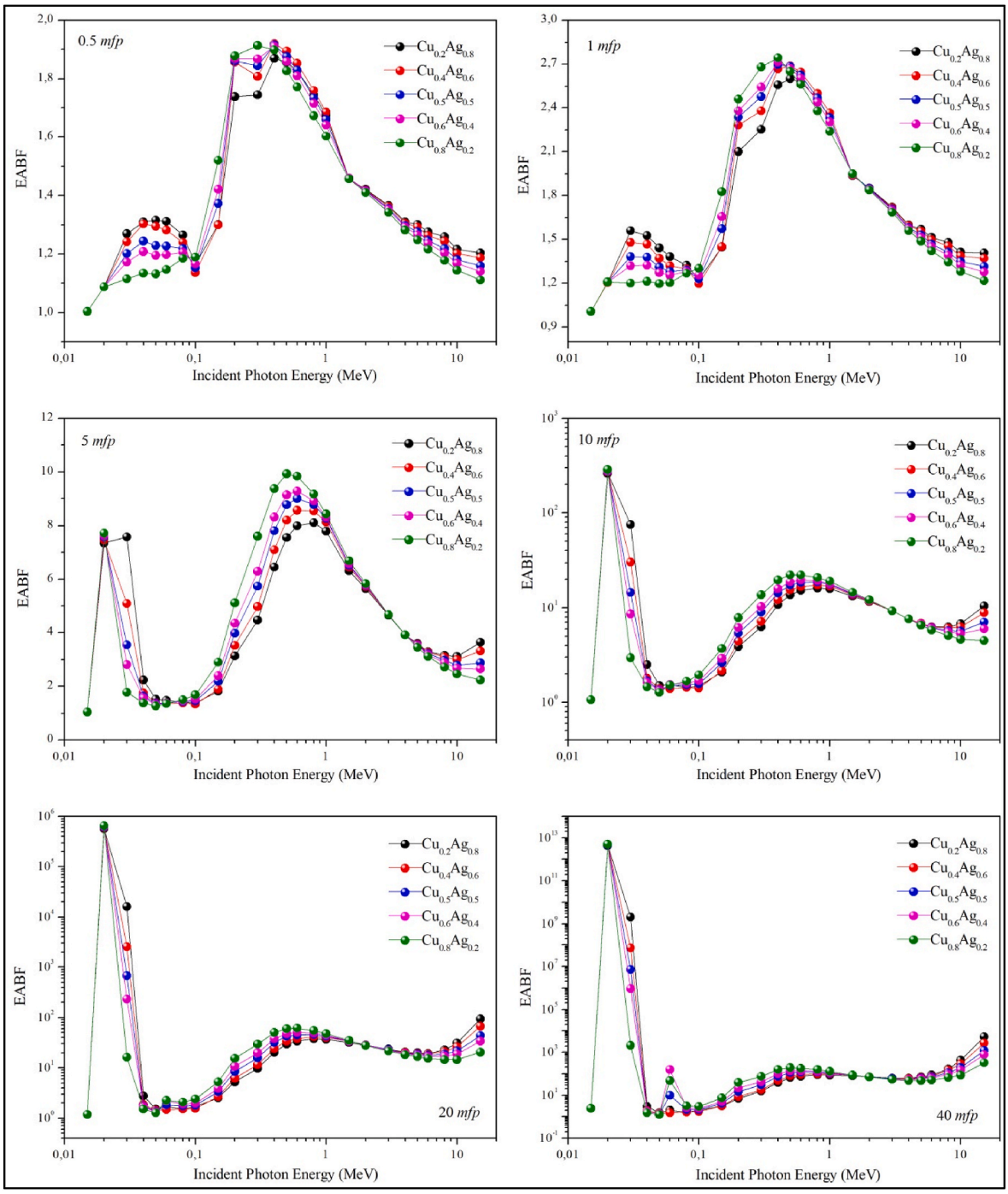

Fig. 6. The energy absorption build-up factor results for fabricated alloys in the energy range of 0.015–15 MeV at 0.5 *mfp*, 1 *mfp*, 5 *mfp*, 10 *mfp*, 20 *mfp* and 40 *mfp*.

coefficient. The numerical experimental and theoretical μ results of the manufactured alloys are given in Table 3. As shown from Table 3, the concentration that has more Ag ($Cu_{0.2}Ag_{0.8}$) has the highest μ values at all given energies comparing to the other concentrations. This shows that the element with higher atomic number (Ag, 47) is better to shield gamma comparing to the element with lower atomic number (Cu, 29). In addition, the difference among the concentrations decreases while the energy is increased. As could be concluded from the provided numerical values, the experimental and theoretical results are close to each other and the μ values of all concentrations decrease, as expected, while the gamma energy increases. *HVL* of a material is defined as the thickness at which the radiation intensity penetrating through the material is reduced to half of its original value. Fig. 3 shows the theoretical *HVL* versus gamma radiation energy results for the prepared alloys. As shown in the figure, the *HVL* increases with the increasing energy for all considered alloys, but the *HVL* shows differences among the prepared alloys. Alloy having more Ag element has higher *HVL* results comparing to the *HVL* results of the other prepared alloys. This also shows that the element with higher atomic number (Ag, 47) is more efficient to keep photons comparing to the element having less atomic number (Cu, 29). While a particle travels through the material, its physical properties such as direction and energy is possible to modify after the particle travels to an average distance. *MFP* is defined as the distance travelled by this particle until its physical properties start to modify. The theoretical *MFP* results for the manufactured alloys are shown in Fig. 4. As can be seen in the figure, the *MFP* increases with the increase of energy. Similar to *HVL*

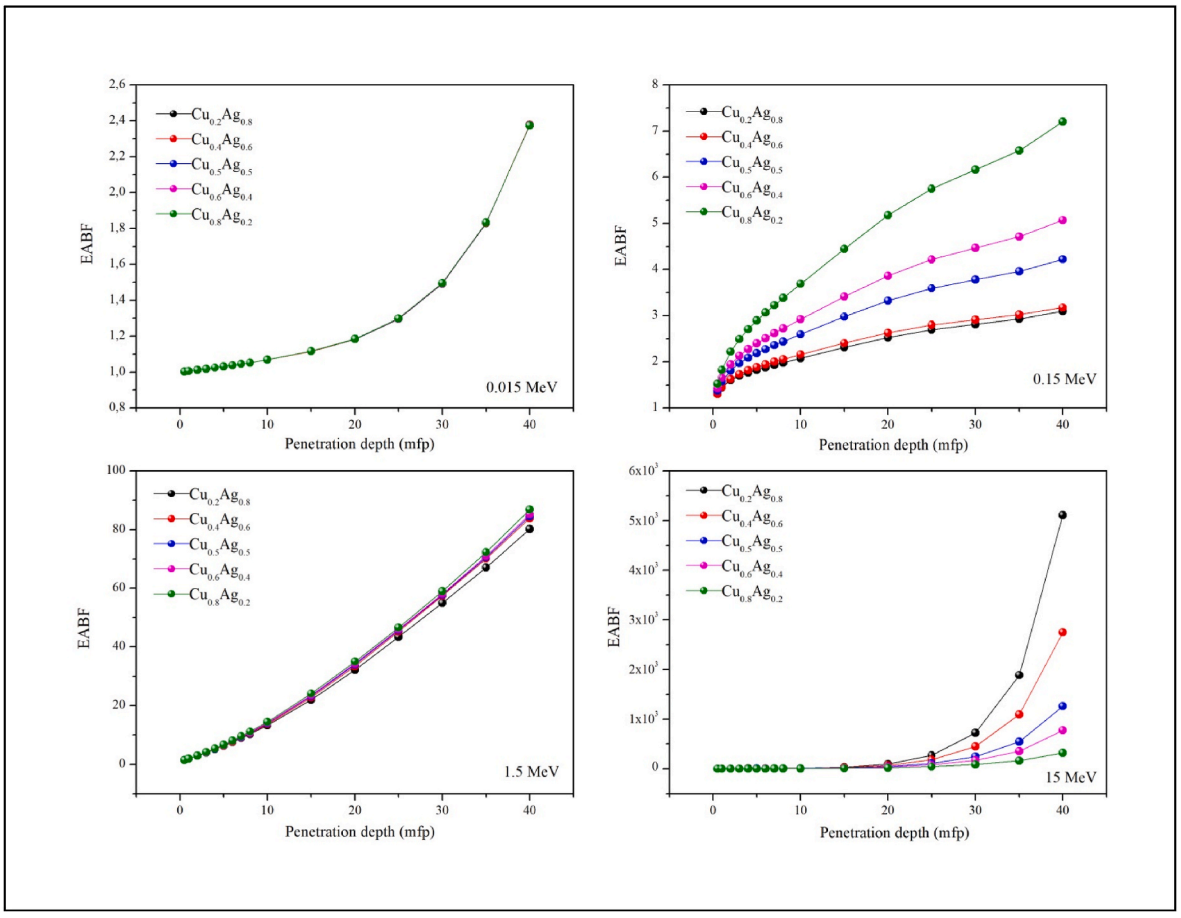

Fig. 7. The energy absorption build-up factor results for synthesized alloys up to 40 *mfp* at 0.015 MeV, 0.15 MeV, 1.50 MeV and 15 MeV photon energies.

results, the concentration having more Ag has higher *MFP* results comparing to the *MFP* results of the concentrations that have less Ag. In addition, the difference among *MFP* results of the manufactured alloys increases with the increasing energy. Moreover, these results are in agreement with those of previously published studies by Alım et al. (2020), Sayyed et al. (2020) and Ozkalayci et al. (2020).

Besides, the *HVL* values of the synthesized alloys are compared to some standard radiation shielding concretes which contain ordinary, hematite– serpentine, ilmenite–limonite, basalt–magnetite, ilmenite, steel–scrap and steel–magnetite (Bashter, 1997), glasses including different oxides (PbO, Bi_2O_3, CdO, Al_2O_3, SiO_2, B_2O_3) (Waly and Fusco, 2016) and some alloys (Akman et al., 2019c) (Fig. 3). The obtained results have lowest values as compared to all concretes (C1–C7) and glasses (S1–S6) while *HVLs* are in line with those of other alloys.

The change of theoretical effective atomic number values versus the photon energy for the manufactured alloys is presented in Fig. 5. The figure clearly shows that the atomic number possess higher values at low energy for the considered alloys due to the fact that the predomination of photoelectric interaction exists in the low energy region. Up to 300 keV, the values were significantly decreased, and then, a slight decrease on the values continued. Besides, with the increase of the Ag amount, a decrease on the Z_{eff} value was observed and remarkable differences for the considered alloys were obtained. In other words, the graph conveys that $Cu_{0.2}Ag_{0.8}$ alloy has better gamma radiation shielding ability.

3.2. Build-up factors

Table 4 gives equivalent atomic numbers of alloys at different energies ranging between 0.015 MeV and 15 MeV while Table 5 presents the numerical values of the G-P *EABF* and *EBF* quantities of the $Cu_{0.4}Ag_{0.6}$ sample at various energy values ranging from 0.015 MeV to 15 MeV. The variations of *EABF* are displayed versus the incident gamma energy varying from 0.015 MeV to 15 MeV at 0.5 *mfp*, 1 *mfp*, 5 *mfp*, 10 *mfp*, 20 *mfp* and 40 *mfp* penetration depths in Fig. 6. Besides, Fig. 7 shows the results for the energy absorption build-up factor as a function of penetration depth (up to 40 *mfp*) at 0.015 MeV, 0.15 MeV, 1.50 MeV and 15 MeV photon energies. Similarly, Figs. 8 and 9 illustrate the exposure build-up factor results as a function of incident photon energy and penetration depths, respectively. It is seen that, at the considered fixed gamma energies, the energy absorption and the exposure build-up factors are increased with increment in the penetration depth. As seen from Figs. 6 and 8, build-up factor values sharply increase up to 20 keV and generally take their maximums in the energy range from 20 keV to 30 keV with increment in the penetration depth. Also, contribution of Ag in the low energy region (especially >20 keV) is clearly seen from Figs. 6 and 8. We can realize this contribution at 30 keV. While build-up factors for $Cu_{0.2}Ag_{0.8}$ of the manufactured alloys take smallest values at 20 keV especially intermediate penetration depths, these values received the highest values (K shell absorption edge energy of Ag is 25.514 keV) at 30 keV for $Cu_{0.2}Ag_{0.8}$ of the manufactured alloys. At 0.015 MeV, *EABF* of the produced alloys versus penetration depth were observed to be similar to each other while the highest *EABF* was found for $Cu_{0.8}Ag_{0.2}$ alloy at 0.15 MeV photon energy. It should be noted here that the differences between the manufactured alloys at 0.15 MeV increase at higher penetration depths. The values of *EABF* versus penetration depth at 0.15 MeV could be ranked as: $Cu_{0.8}Ag_{0.2}$ > $Cu_{0.6}Ag_{0.4}$ > $Cu_{0.5}Ag_{0.5}$ > $Cu_{0.4}Ag_{0.6}$ > $Cu_{0.2}Ag_{0.8}$. Compared to the results of alloys at 0.15 MeV, the variance between the build-up factor values of the produced materials were found to be smaller but $Cu_{0.8}Ag_{0.2}$ alloy also had the highest *EABF* value. At 15 MeV gamma ray energy, the

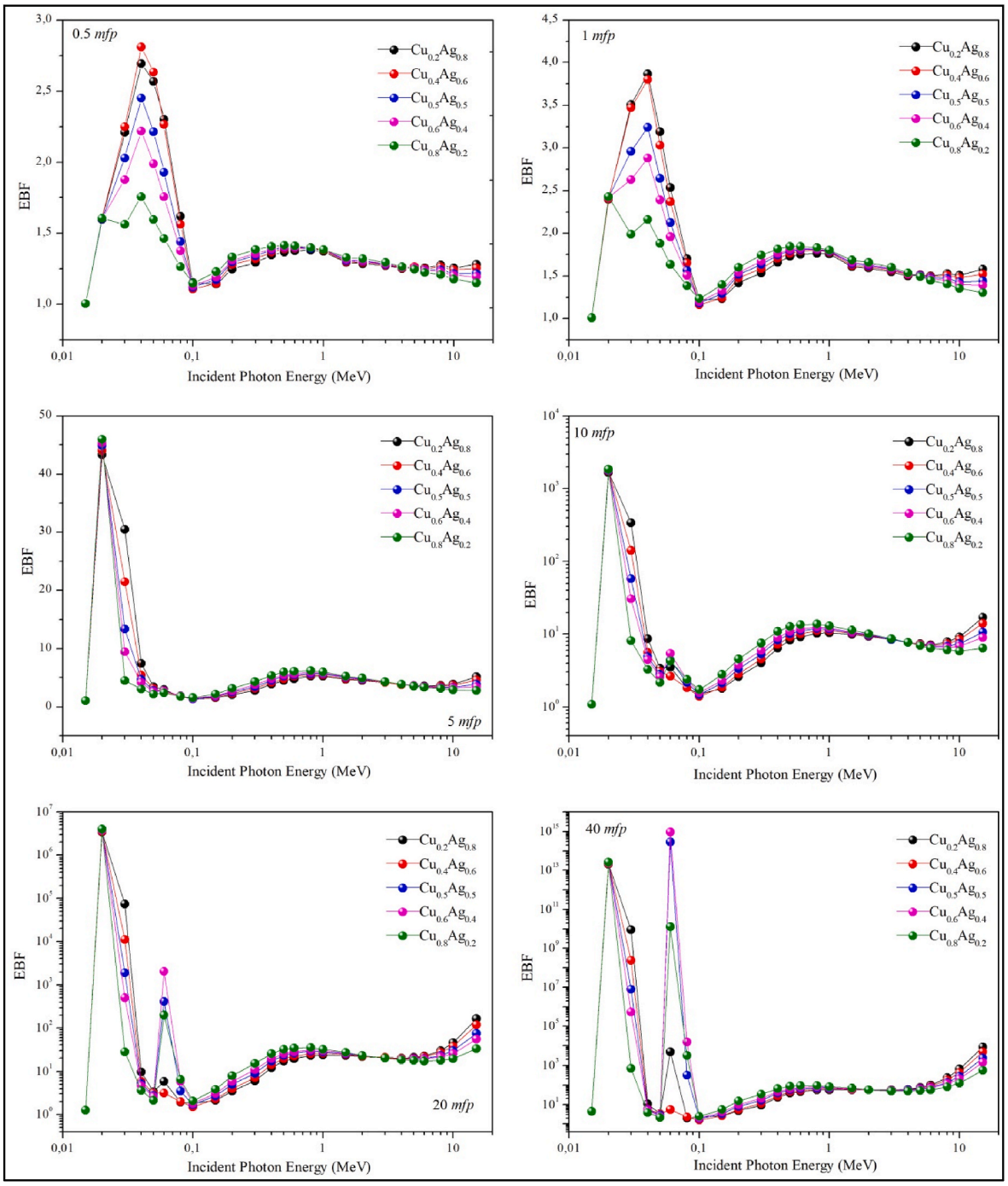

Fig. 8. The exposure build-up factor results for alloys under investigation in the energy range of 0.015–15 MeV at 0.5 *mfp*, 1 *mfp*, 5 *mfp*, 10 *mfp*, 20 *mfp* and 40 *mfp*.

alloys have similar and nearly constant *EABF* values up to the penetration depth of 20 *mfp*. They were then separated after that point. At this high energy, the values of *EABF* could be listed as: $Cu_{0.8}Ag_{0.2}$ < $Cu_{0.6}Ag_{0.4}$ < $Cu_{0.5}Ag_{0.5}$ < $Cu_{0.4}Ag_{0.6}$ < $Cu_{0.2}Ag_{0.8}$, and the difference between the alloys was the highest at 40 *mfp*. Similar behavior to *EABF* graphs was also obtained in the graphs of *EBF*; therefore, all comments made for *EABF* figures are also valid for *EBF* results.

3.3. Kerma relative to air

Kerma is a quantity which is generally defined for ionizing radiation and transfers energy from uncharged particles, such as photon, to the material. The kerma relative to air of the manufactured alloys is calculated for the photon energy ranges from 1 keV to 20 MeV. Fig. 10 shows the kerma relative to air values as a function of energy for the manufactured alloys. As seen from Fig. 10, kerma relative to air values increased with increasing photon energy up to ~350 keV. Also, the values of kerma relative to air showed sharp increases and then decreases in some energy points (Cu and Ag K shell and L sub-shells absorption edge) this lower energy region. As a result of fluctuations, sawtooth structures were formed. Reduction of the kerma relative to air values are observed in the intermediate energy region and then the values showed an inverted trend in the high energy region and $Cu_{0.2}Ag_{0.8}$ took the highest kerma relative to air values just like *EABF* and *EBF* values at especially penetration depth 20 *mfp* ≤ PD ≤ 40 *mfp*. This situation can be explain that pair production is more dominant in

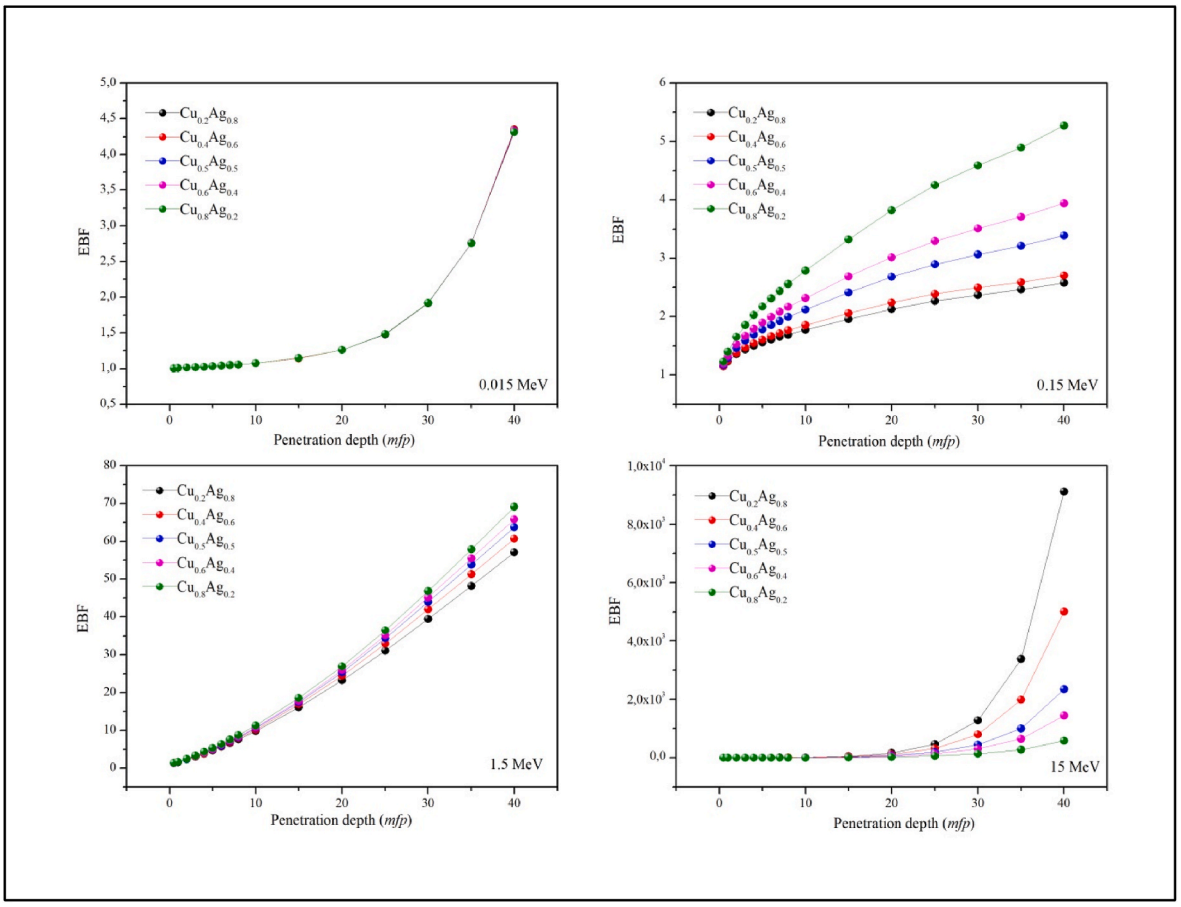

Fig. 9. The exposure build-up factor results for the studied alloys up to 40 *mfp* at 0.015 MeV, 0.15 MeV, 1.50 MeV and 15 MeV photon energies.

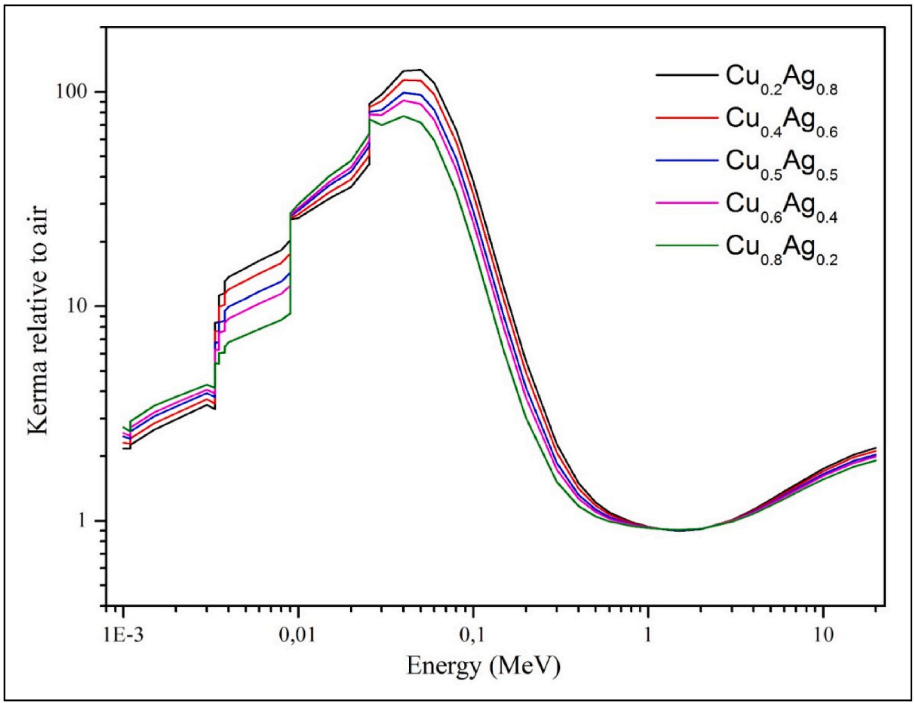

Fig. 10. The variation of photon energy versus kerma relative to air for the manufactured alloys.

the high energy region and as mentioned above pair production is approximately dependent on Z^2.

4. Conclusions

μ/ρ, μ, *HVL*, *MFP* and Z_{Eff} were determined in the energy range from 59.5 keV to 1332.5 keV for different binary alloys such as $Cu_{0.2}Ag_{0.8}$, $Cu_{0.4}Ag_{0.6}$, $Cu_{0.5}Ag_{0.5}$, $Cu_{0.6}Ag_{0.4}$ and $Cu_{0.8}Ag_{0.2}$. *EABF* and *EBF* values were calculated in the energy region 0.015 MeV $\leq$ E $\leq$ 15 MeV for penetration depths up to 40 *mfp* for binary alloys. Also, kerma relative to air values for the binary alloys were investigated in the energy region 0.001 MeV $\leq$ E $\leq$ 20 MeV. The experimental results of mass attenuation coefficients are in line with those of WinXCOM, FLUKA and GEANT4 ones. Other related shielding parameters depending on photon energies namely effective atomic number and exposure buildup factor (above 5 MeV) increase with the increment in Ag amount in the binary alloys. Also, all parameters appeared to support each other for each binary alloy. As shown in tables and figures, $Cu_{0.2}Ag_{0.8}$ is a good radiation absorber according to the other studied binary alloys and it can be offered an alternative shielding material against gamma radiations among the studied binary alloys. Because the number of studies is very limited in the literature for the attenuation parameters on binary alloys, the feasibility of various alloys with some high-Z element can be investigated in detail for its liable application in designing shield high energetic photon. In addition to attenuation parameters, other significant requirements should be discussed by linking to structural and mechanical characterizations. The present results may contribute to various application areas of radiation research especially engineering areas.

Declaration of competing interest

No potential conflict of interest was reported by the authors.

Acknowledgements

None.

References

Agar, O., Boztosun, I., Segebade, C., 2017. Multielemental analysis of some soils in Karaman by PAA using a cLINAC. Appl. Radiat. Isot. 122, 57–62.

Agar, O., Sayyed, M.I., Akman, F., Tekin, H.O., Kaçal, M.R., 2019. An extensive investigation on gamma ray shielding features of Pd/Ag-based alloys. Nucl. Eng. Tech. 51 (3), 853–859.

Agostinelli, S., Allison, J., Amako, K.A., Apostolakis, J., Araujo, H., Arce, P., Asai, M., Axen, D., Banerjee, S., Barrand, G.2., Behner, F., 2003. Geant4 Collaboration. GEANT4—a simulation toolkit. Nucl. Instrum. Methods Phys. Res., Sect. A 506 (3), 250–303.

Ahmed, T., Flower, H.M., 1992. The Phase Transformations in Alloys Based on Titanium Aluminides Ti3Al–V and TiAl–V. Elsevier, High Temperature Aluminides and Intermetallics, pp. 31–36.

Akman, F., Geçibesler, I.H., Sayyed, M.I., Tijani, S.A., Tufekci, A.R., Demirtas, I., 2018. Determination of some useful radiation interaction parameters for waste foods. Nucl. Eng. Tech. 50 (6), 944–949.

Akman, F., Khattari, Z.Y., Kaçal, M.R., Sayyed, M.I., Afaneh, F., 2019a. The radiation shielding features for some silicide, boride and oxide types ceramics. Radiat. Phys. Chem. 160, 9–14.

Akman, F., Agar, O., Kaçal, M.R., Sayyed, M.I., 2019b. Comparison of experimental and theoretical radiation shielding parameters of several environmentally friendly materials. Nucl. Sci. Tech. 30 (7), 1–8.

Akman, F., Kaçal, M.R., Sayyed, M.I., Karataş, H.A., 2019c. Study of gamma radiation attenuation properties of some selected ternary alloys. J. Alloys Compd. 782, 315–322.

Akman, F., Ogul, H., Kaçal, M.R., Polat, H., Dilsiz, K., Turhan, M.F., 2020. Impact of lead (II) iodide on radiation shielding properties of polyester composites. Appl. Phys. A 126 (4), 1–9.

Akman, F., Ozkan, I., Kaçal, M.R., Polat, H., Issa, S.A., Tekin, H.O., Agar, O., 2021a. Shielding features, to non-ionizing and ionizing photons, of FeCr-based composites. Appl. Radiat. Isot. 167, 109470.

Akman, F., Ogul, H., Kaçal, M.R., Polat, H., Dilsiz, K., Agar, O., 2021b. Gamma attenuation characteristics of CdTe-Doped polyester composites. Prog. Nucl. Energy 131, 103608.

Akman, F., Kaçal, M.R., Polat, H., Aktas, G., Gultekin, A., Agar, O., 2021c. A comparative study on the nuclear shielding properties of BiBr3 and PbSO4 incorporated composites. J. Phys. Chem. Solid. 152, 109978.

Al-Buriahi, M.S., Singh, V.P., 2020. Comparison of shielding properties of various marble concretes using GEANT4 simulation and experimental data. J. Australas. Ceram. Soc. 56, 1127–1133.

Al-Buriahi, M.S., Gaikwad, D.K., Hegazy, H.H., Sriwunkum, C., Neffati, R., 2021. Fe-based alloys and their shielding properties against directly and indirectly ionizing radiation by using FLUKA simulations. Phys. Scripta 96 (4), 045303.

Alım, B., Şakar, E., Baltakesmez, A., Han, İ., Sayyed, M.I., Demir, L., 2020. Experimental investigation of radiation shielding performances of some important AISI-coded stainless steels: Part I. Radiat. Phys. Chem. 166, 108455.

Almatari, M., Agar, O., Altunsoy, E.E., Kilicoglu, O., Sayyed, M.I., Tekin, H.O., 2019. Photon and neutron shielding characteristics of samarium doped lead alumino borate glasses containing barium, lithium and zinc oxides determined at medical diagnostic energies. Results Phys 12, 2123–2128.

ANSI/ANS-6.4.3., 1991. American Nuclear Society, La Grange Park, IL, USA.

Aşkin, A., Mutuwong, C., Nutaro, T., Dal, M., 2020. Investigation of the radiation shielding capability of xPbO–(50-x)BaO–50B2O3 glass system using Geant4, Fluka, WinXCOM and comparison of data with the experimental data. Pramana - J. Phys. 94 (1), 1–7.

Aygün, B., Şakar, E., Cinan, E., Yorgun, N.Y., Sayyed, M.I., Agar, O., Karabulut, A., 2020. Development and production of metal oxide doped glasses for gamma ray and fast neutron shielding. Radiat. Phys. Chem. 174, 108897.

Bashter, I., 1997. Calculation of radiation attenuation coefficients for shielding concretes. Ann. Nucl. Energy 24, 1389–1401.

Boztosun, İ., Dapo, H., Özmen, S.F., Çeçen, Y., Karakoç, M., Çoban, A., Cesur, A., Caner, T., Bayram, E., Keller, G.B., Küçük, B., Güvendi, A., Derman, M., Kaya, D., 2014. The results of the first photonuclear reaction performed in Turkey: the zinc example. Turk. J. Phys. 38 (1), 1–9.

Böhlen, T.T., Cerutti, F., Chin, M.P.W., Fassò, A., Ferrari, A., Ortega, P.G., Mairani, A., Sala, P.R., Smirnov, G., Vlachoudis, V., 2014. The FLUKA code: developments and challenges for high energy and medical applications. Nucl. Data Sheets 120, 211–214.

Eke, C., Agar, O., Segebade, C., Boztosun, I., 2017. Attenuation properties of radiation shielding materials such as granite and marble against γ-ray energies between 80 and 1350 keV. Radiochim. Acta 105 (10), 851–863.

Elbashir, B.O., Dong, M.G., Sayyed, M.I., Issa, S.A.M., Matori, K.A., Zaid, M.H.M., 2018. Comparison of Monte Carlo simulation of gamma ray attenuation coefficients of amino acids with XCOM program and experimental data. Results Phys 9, 9–11.

Gerward, L., Guilbert, N., Jensen, K.B., Levring, H., 2004. WinXCom—a program for calculating X-ray attenuation coefficients. Radiat. Phys. Chem. 71 (3–4), 653–654.

Hamad, R.M., Mhareb, M.H.A., Alajerami, Y.S., Sayyed, M.I., Saleh, G., Hamad, M.K., Ziq, K., 2021. A comprehensive ionizing radiation shielding study of FexSe0. 5Te0. 5 alloys with various iron concentrations. J. Alloys Compd. 858, 157636.

Hubbell, J.H., Seltzer, S.M., 1995. Tables of X-Ray Mass Attenuation Coefficients and Mass Energy-Absorption Coefficients 1 keV to 20 MeV for Elements Z= 1 to 92 and 48 Additional Substances of Dosimetric Interest. National Institute of Standards and Physics Laboratory, NISTIR, p. 5632.

Kaçal, M.R., Polat, H., Oltulu, M., Akman, F., Agar, O., Tekin, H.O., 2020. Gamma shielding and compressive strength analyses of polyester composites reinforced with zinc: an experiment, theoretical, and simulation based study. Appl. Phys. A 126 (3), 1–15.

Kaçal, M.R., Dilsiz, K., Akman, F., Polat, H., 2021. Analysis of radiation attenuation properties for Polyester/Li2WO4 composites. Radiat. Phys. Chem. 179, 109257.

Kamal, M., Moharram, B.M., Farag, H., El-Bediwi, A., Abosheiasha, H.F., 2006. Structure, attenuation coefficients and physical properties of Bi–Pb–Sn fusible alloys. Radiat. Eff. Defect Solid 161 (2), 137–142.

Kaur, T., Sharma, J., Singh, T., 2019. Review on scope of metallic alloys in gamma rays shield designing. Progr. Nuclear Energy 113, 95–113.

Kok, B., Benli, H., 2017. Energy diversity and nuclear energy for sustainable development in Turkey. Renew. Energy 111, 870–877.

Kurtulus, R., Kavas, T., Akkurt, I., Gunoglu, K., Tekin, H.O., Kurtulus, C., 2021. A comprehensive study on novel alumino-borosilicate glass reinforced with Bi2O3 for radiation shielding applications: synthesis, spectrometer, XCOM, and MCNP-X works. J. Mater. Sci. Mater. Electron. 32, 13882–13896.

Levet, A., Kavaz, E., Özdemir, Y., 2020. An experimental study on the investigation of nuclear radiation shielding characteristics in iron-boron alloys. J. Alloys Compd. 819, 152946.

Majid, J., Mohammad, R., Mojtaba, M., 2013. Prompt gamma radiation as a new tool to measure reactor power. Radiat. Phys. Chem. 91, 19–27.

Moiseev, V.N., Sysoeva, N.V., Polyakova, I.G., 1998. Effect of additional carbon and boron alloying on the structure and mechanical properties of alloy VT22. Met. Sci. Heat treat. 40 (3), 107–111.

Özkalaycı, F., Kaçal, M.R., Agar, O., Polat, H., Sharma, A., Akman, F., 2020. Lead (II) chloride effects on nuclear shielding capabilities of polymer composites. J. Phys. Chem. Solid. 145, 109543.

Reda, A.M., El-Daly, A.A., 2020. Gamma ray shielding characteristics of Sn-20Bi and Sn-20Bi-0.4 Cu lead-free alloys. Prog. Nucl. Energy 123, 103304.

Sayyed, M.I., Akman, F., Kumar, A., Kaçal, M.R., 2018. Evaluation of radioprotection properties of some selected ceramic samples. Results Phys 11, 1100–1104.

Sayyed, M.I., Tekin, H.O., Agar, O., 2019. Gamma photon and neutron attenuation properties of MgO–BaO–B2O3–TeO2–Cr2O3 glasses: the role of TeO2. Radiat. Phys. Chem. 163, 58–66.

Sayyed, M.I., Agar, O., Kumar, A., Tekin, H.O., Gaikwad, D.K., Obaid, S.S., 2020. Shielding behaviour of (20+ x) Bi2O3–20BaO–10Na2O–10MgO–(40-x) B2O3: an experimental and Monte Carlo study. Chem. Phys. 529, 110571.
Sharma, A., Sayyed, M.I., Agar, O., Kaçal, M.R., Polat, H., Akman, F., 2020. Photon-shielding performance of bismuth oxychloride-filled polyester concretes. Mater. Chem. Phys. 241, 122330.
Singh, J., Singh, H., Sharma, J., Singh, T., Singh, P.S., 2018. Fusible alloys: a potential candidate for gamma rays shield design. Prog. Nucl. Energy 106, 387–395.
Suortti, P., Thomlinson, W., 2003. Medical applications of synchrotron radiation. Phys. Med. Biol. 48 (13), R1.
Taqi, A.H., Ghalib, A.M., Mohammed, H.N., 2021. Shielding properties of Cu-Sn-Pb alloy by Geant4, XCOM and experimental data. Mater. Today Commun. 26, 101996.
Tekin, H.O., Kilicoglu, O., 2020. The influence of gallium (Ga) additive on nuclear radiation shielding effectiveness of Pd/Mn binary alloys. J. Alloys Compd. 815, 152484.
Tellili, B., Elmahroug, Y., Souga, C., 2017. Investigation on radiation shielding parameters of cerrobend alloys. Nucl. Eng. Technol. 49 (8), 1758–1771.
Waly, E.S.A., Fusco, M.A., Bourham, M.A., 2016. Gamma-ray mass attenuation coefficient and half value layer factor of some oxide glass shielding materials. Ann. Nucl. Energy 96, 26–30.